Inorg. Chem. **2002**, *41*, 4424–4434

Density Functional Calculations for Modeling the Active Site of Nickel–Iron Hydrogenases. 2. Predictions for the Unready and Ready States and the Corresponding Activation Processes

Christian Stadler,[†] Antonio L. de Lacey,[†] Yael Montet,[‡] Anne Volbeda,[‡] Juan C. Fontecilla-Camps,[‡] Jose C. Conesa,*[,†] and Víctor M. Fernández*[,†]

Instituto de Catálisis, CSIC, Campus Universidad Autónoma, 28049 Madrid, Spain, and Laboratoire de Cristallographie et Cristallogenèse des Protéines, IBS "J.-P. Ebel" CEA-CNRS, Grenoble Cedex 1, France

Received January 4, 2002

ZORA relativistic DFT calculations are presented which aim to model the geometric and electronic structure of the active site of NiFe hydrogenases in its EPR-active oxidized states Ni-A (unready state) and Ni-B (ready state). Starting coordinates are taken from the X-ray structure of a mutant of *Desulfovibrio fructosovorans* hydrogenase refined at 1.81 Å resolution. Nine possible candidates for Ni-A and Ni-B are analyzed in terms of their geometric and electronic structure. Comparison of calculated geometric and magnetic resonance parameters with available experimental data indicates that both oxidized states have a μ-hydroxo bridge between the two metal centers. The different electronic structures of both forms can be explained by a modification of a terminal cysteine in Ni-B, best modeled by protonation of the sulfur atom. A possible mechanism for the activation of both oxidized forms is presented.

Introduction

Hydrogenases are enzymes that catalyze the reversible oxidation of molecular hydrogen. The most studied representatives are those that contain a redox active nickel ion and several iron atoms.[1] These NiFe hydrogenases show an exceptionally rich electrochemistry with at least six spectroscopically distinguishable redox states participating in the activation/inactivation processes and the catalytic cycle.[2] The X-ray crystallographic structure of aerobically purified *Desulfovibrio gigas* hydrogenase indicates that the active site is composed of a bimetallic NiFe center bridged by two thiolates (from cysteine residues) and an oxygen species.[3] Two more cysteines are coordinated to the Ni center, whereas the Fe atom has three diatomic ligands. These have been identified by FTIR spectroscopy as two cyanides and one carbonyl group.[4] Recently, several more crystallographic structures of different NiFe hydrogenases in oxidized[5] and reduced[6] states have been reported. Despite this progress and the huge amount of available spectroscopic and kinetic data, many aspects of the enzyme operation mechanism and the underlying electronic structure features are ill understood. Therefore, their elucidation by theoretical methods is of great interest. Several density functional (DFT) studies on the active site of these enzymes have been published recently.[7]

* To whom correspondence should be addressed. E-mail: vmfernandez@icp.csic.es (V.M.F.); jcconesa@icp.csic.es (J.C.C.).
[†] Campus Universidad Autónoma.
[‡] IBS "J.-P. Ebel" CEA-CNRS.

(1) (a) Cammack, R.; Fernandez, V. M.; Schneider, K. In *The Bioinorganic Chemistry of Nickel*; Lancaster, J. R., Jr., Ed.; VCH: Weinheim, 1988; pp 167−190. (b) Moura, J. J. G.; Teixeira, M.; Moura, I.; LeGall, J. In *The Bioinorganic Chemistry of Nickel*; Lancaster, J. R., Jr., Ed.; VCH: Weinheim, 1988; pp 191−226. (c) Albracht, S. P. J. *Biochim. Biophys. Acta* **1994**, *1188*, 167−204.
(2) De Lacey, A. L.; Hatchikian, E. C.; Volbeda, A.; Frey, M.; Fontecilla-Camps, J. C.; Fernandez, V. M. *J. Am. Chem. Soc.* **1997**, *119*, 7181−7189.
(3) (a) Volbeda, A.; Charon, M. H.; Piras, C.; Hatchikian, E. C.; Frey, M.; Fontecilla-Camps, J. C. *Nature* **1995**, *373*, 580−587. (b) Volbeda, A.; Garcin, E.; Piras, C.; De Lacey, A. L.; Fernandez, V. M.; Hatchikian, E. C.; Frey, M.; Fontecilla-Camps, J. C. *J. Am. Chem. Soc.* **1996**, *118*, 12989−12996.
(4) (a) Happe, R. P.; Roseboom, W.; Pierik, A. J.; Albracht, S. P. J.; Bagley, K. A. *Nature* **1997**, *385*, 126. (b) Pierik, A. J.; Roseboom, W.; Happe, R. P.; Bagley, K. A.; Albracht, S. P. J. *J. Biol. Chem.* **1999**, *274*, 3331−3337.
(5) (a) Higuchi, Y.; Yagi, T.; Yasuoka, N. *Structure* **1997**, *5*, 1671−1680. (b) Matias, P. M.; Soares, C. M.; Saraiva, L. M.; Coelho, R.; Morais, J.; Le Gall, J.; Carrondo, A. M. *J. Biol. Inorg. Chem.* **2001**, *6*, 63−81.
(6) (a) Higuchi, Y.; Ogata, H.; Miki, K.; Yasuoka, N.; Yagi, T. *Structure* **1999**, *7*, 549−556. (b) Garcin, E.; Vernede, X.; Hatchikian, C.; Volbeda, A.; Frey, M.; Fontecilla-Camps, J. C. *Structure* **1999**, *7*, 557−566.

10.1021/ic020016l CCC: $22.00
Published on Web 07/31/2002

However, the various computational models differ considerably, and the detailed reaction mechanism still remains a matter of debate.[8]

One crucial step for the successful modeling of the NiFe hydrogenases' reaction mechanism is the correct description of the oxidized states Ni-A and Ni-B, which are the structurally and spectroscopically best characterized states. Consequently, they are most frequently used as the starting models in theoretical studies. Both Ni-A and Ni-B are generally considered Ni(III) states and were originally differentiated by EPR spectroscopy[9] and by their kinetic behavior.[10] Though both of them are catalytically inactive and, apparently, structurally very similar, Ni-B (also named ready state) quickly becomes active upon reduction whereas Ni-A (unready state) needs a long activation process under reducing conditions.[10] It is crucial for the understanding of the activation/deactivation processes to determine which structural changes cause the different kinetic behavior. In particular, the protonation states of Ni-A and Ni-B, which are not known from crystallography, have to be determined. This would also greatly help the proper modeling of the other states participating in the active cycle, making use of the known redox and protonation equilibria between the different states.[2] Some of the best characterized properties of these enzymes are the parameters obtained by EPR (and ENDOR) spectroscopy, for example, the *g*-values[9] and the *g*-tensor orientation.[11] Moreover, they are very closely related to the active site's electronic structure and are expected to depend sensitively on the protonation state. Therefore, a computational method that focuses on the modeling of EPR parameters should be better suited for the determination of the apparently small structural differences between Ni-A and Ni-B than other methods focusing on energetics of hydrogen activation[7a,b,e] or infrared frequencies of the diatomic ligands bound to the Fe center.[7e−g]

In the accompanying work, we have tested such a computational method for calculating *g*-values, hyperfine coupling, and ^{14}N quadrupole coupling with paramagnetic Ni and Co complexes.[12] Comparison of calculated and experimental parameters has allowed us to calibrate the method in order to perform calculations on models of the active site of NiFe hydrogenases. In this work, results obtained for several models of the oxidized enzyme states Ni-A and Ni-B of NiFe hydrogenases are presented. In particular, the nature of the bridging oxygen species and possible structural differences between these two states are discussed. The most likely models are then integrated into an overall scheme that may explain the different mechanisms of activation of Ni-A and Ni-B.

Methods and Models

All calculations were done with the Amsterdam density functional (ADF) program package[13] using Slater-type orbitals and the ZORA (zeroth-order regular approximation) relativistic method.[14] The computational details are described in an accompanying paper.[12] Dielectric effects were calculated with the ADF implementation of COSMO (conductor screening model) which puts the molecule in a cavity surrounded by a dielectric continuum.[15] Default values for the radii of different atom types were used for the generation of the cavity.[16] To model the protein environment of the hydrogenase active site, the dielectric constant was chosen to be equal to 4 as proposed in the literature.[7b,17]

The calculations on models of the hydrogenase active site are based on experimental coordinates that have been taken from a recent X-ray structure of a mutant of *Desulfovibrio fructosovorans* hydrogenase. The crystal structure has been determined to a resolution of 1.81 Å.[18] The mutation, which consists of the replacement of Ser499 by an Ala, does not give rise to significant functional or spectroscopic changes, and consequently, the EPR and IR spectra of this mutant and of native *D. gigas* and *D. fructosovorans* hydrogenases are practically identical.[19] The refined structure agrees very well with the observed data. The crystallographic *R*-factor, defined as $\sum_{hkl}|F_{obs}(h,k,l) - F_{calcd}(h,k,l)|/\sum_{hkl}F_{obs}(h,k,l)$, is 14.9%, whereas R_{free} is 18.7%, using, respectively, 95% and 5% of all observations up to 1.81 Å resolution. The root-mean-square deviations with respect to dictionary values of bond distances and angles for all amino acid residues are 0.007 Å and 1.4°, respectively. The structure of the active site is close to the one described for *D. gigas* NiFe hydrogenase, which is thought to correspond mainly to the Ni-A state.[3b] Accordingly, the percentage of Ni-A in the enzyme preparations of the mutant is typically more than 80% as determined by FTIR spectroscopy. A small difference is obtained for the position of the bridging oxygen ligand, which was reported to be at 1.7 Å from the Ni in the 2.5 Å resolution *D.*

(7) (a) Pavlov, M.; Siegbahn, P. E. M.; Blomberg, M. R. A.; Crabtree, R. H. *J. Am. Chem. Soc.* **1998**, *120*, 548−555. (b) Pavlov, M.; Blomberg, M. R. A.; Siegbahn, P. E. M. *Int. J. Quantum Chem.* **1999**, *73*, 197−207. (c) De Gioia, L.; Fantucci, P.; Guigliarelli, B.; Bertrand, P. *Inorg. Chem.* **1999**, *38*, 2658−2662. (d) De Gioia, L.; Fantucci, P.; Guigliarelli, B.; Bertrand, P. *Int. J. Quantum Chem.* **1999**, *73*, 187−195. (e) Niu, S.; Thomson, L. M.; Hall, M. B. *J. Am. Chem. Soc.* **1999**, *121*, 4000−4007. (f) Amara, P.; Volbeda, A.; Fontecilla-Camps, J. C.; Field, M. J. *J. Am. Chem. Soc.* **1999**, *121*, 4468−4477. (g) Li, S.; Hall, M. B. *Inorg. Chem.* **2001**, *40*, 18−24. (h) Stein, M.; Van Lenthe, E.; Baerends, E. J.; Lubitz, W. *J. Am. Chem. Soc.* **2001**, *123*, 5839−5840. (i) Stein, M.; Lubitz, W. *Phys. Chem. Chem. Phys.* **2001**, *3*, 2668−2675. (j) Niu, S.; Hall, M. B. *Inorg. Chem.* **2001**, *40*, 6201−6203.

(8) Maroney, M. J.; Bryngelson, P. A. *J. Biol. Inorg. Chem.* **2001**, *6*, 453−459.

(9) (a) Moura, J. J. G.; Moura, I.; Huynh, B.-H.; Krüger, H. J.; Teixeira, M.; DuVarney, R. C.; DerVartanian, D. V.; Xavier, A. V.; Peck, H. D., Jr.; LeGall, J. *Biochem. Biophys. Res. Commun.* **1982**, *108*, 1388−1393. (b) Cammack, R.; Patil, O. S.; Hatchikian, E. C.; Fernandez, V. M. *Biochim. Biophys. Acta* **1987**, *912*, 98−109.

(10) (a) Fernandez, V. M.; Hatchikian, E. C.; Cammack, R. *Biochim. Biophys. Acta* **1985**, *832*, 69−79. (b) Fernandez, V. M.; Rao, K. K.; Fernandez, M. A.; Cammack, R. *Biochimie* **1986**, *68*, 43−48.

(11) Trofanchuk, O.; Stein, L.; Gessner, C.; Lendzian, F.; Higuchi, Y.; Lubitz, W. *J. Biol. Inorg. Chem.* **2000**, *5*, 36−44.

(12) See companion paper: Stadler, C.; De Lacey, A. L.; Hernandez, B.; Conesa, J. C.; Fernandez, V. M. *Inorg. Chem.* **2002**, *41*, 4417−4423.

(13) (a) ADF 1999.02 and ADF 2000.02. (b) Fonseca Guerra, C.; Snijders, J. G.; Te Velde, G.; Baerends, E. J. *Theor. Chem. Acc.* **1998**, *99*, 391−403.

(14) Van Lenthe, E.; Snijders, J. G.; Baerends, E. J. *J. Chem. Phys.* **1996**, *105*, 6505−6516. (b) Van Lenthe, E.; Ehlers, A.; Baerends, E. J. *J. Chem. Phys.* **1999**, *110*, 8943−8953.

(15) Pye, C. C.; Ziegler, T. *Theor. Chem. Acc.* **1999**, *101*, 396−408.

(16) 1.18 Å for H, 1.63 Å for C, 1.58 Å for N, 1.46 Å for O, 1.80 Å for S, 1.26 Å for Fe, and 1.24 Å for Ni.

(17) Siegbahn, P. E. M.; Blomberg, M. R. A. *Chem. Rev.* **2000**, *100*, 421−437.

(18) (a) Montet-Bertheas, Y. Ph.D. Thesis, Université Joseph Fourier, Grenoble, France, 1998. (b) Volbeda et al. Manuscript in preparation.

(19) (a) Hatchikian, E. C.; Traore, A. S.; Fernandez, V. M.; Cammack, R. *Eur. J. Biochem.* **1990**, *187*, 635−643. (b) De Lacey, A. L.; Stadler, C.; Fernandez, V. M.; Hatchikian, E. C.; Fan, H.-J.; Li, S.; Hall, M. B. *J. Biol. Inorg. Chem.* **2002**, *7*, 318−326.

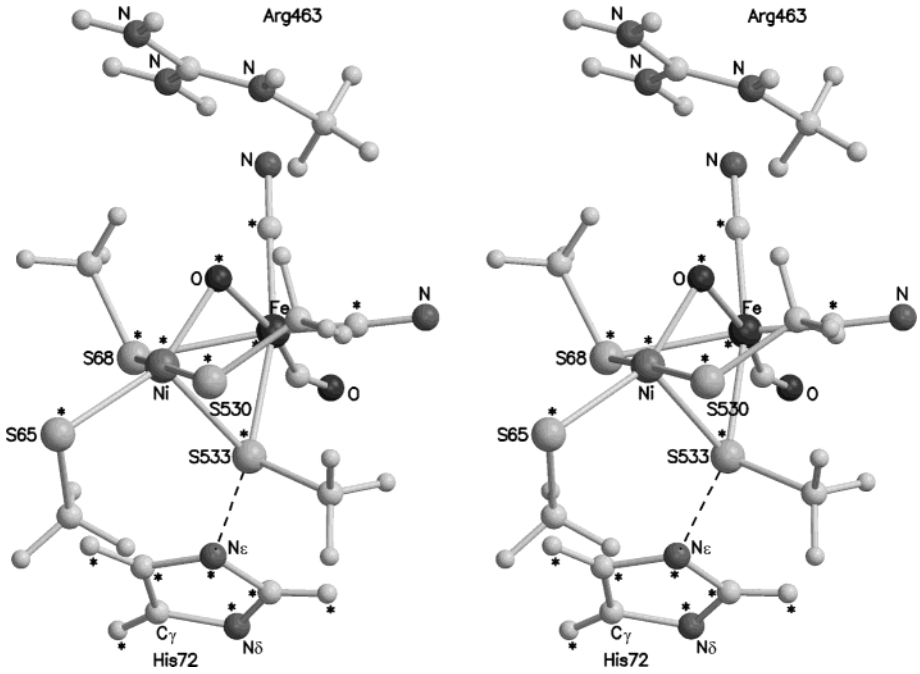

Figure 1. Stereoview (crossed eyes) of the crystallographically determined structure of the active site of the hydrogenase from *D. fructosovorans* (mutant Ser499Ala) as used in the calculations. The guanido group of Arg463 is included in both the basic and the extended models whereas the imidazole ring of His72 is only present in the latter. Atoms allowed to move in the geometry optimization are marked by an asterisk.

gigas enzyme model. This ligand refines here to a distance of 1.9 Å to the Ni. In addition, a second conformation of Cys543 (Cys530 in *D. gigas*) is found. A conformational flexibility of the same residue has also been observed in the structure of an oxidized form of *D. desulfuricans* NiFe hydrogenase.[5b]

For our calculations we used two models of different size; the larger one is shown in Figure 1. The smaller *basic model* consists of the dinuclear cluster (including all direct ligands to Ni and Fe) and the guanido group of an arginine residue that is close to the cluster, whereas the *extended model* also includes the imidazole ring of a nearby histidine residue. The four cysteine residues are modeled as $S-CH_3$ groups, and the guanido group is assumed to be protonated, in accordance with its rather high pK_a value.[20] We would like to point out that a bigger model with $S-CH_2-CH_3$ moieties gave very similar results although this has been doubted recently.[7h] However, we agree with these authors insofar that SH groups are absolutely insufficient to describe the active site. To facilitate comparison with other published work, the numbering scheme of *D. gigas* hydrogenase is used for the amino acid residues throughout the paper.

Prior to calculations of *g*-tensors and hyperfine couplings, all structures were energy-minimized, but several constraints were applied to prevent the models from unlikely structural changes. Only atoms marked with an asterisk (Figure 1), plus any protons bound to them, are included in the geometry optimization, whereas all other atoms are kept fixed at their experimentally determined position. Although the actual constraints imposed by the protein backbone may be less rigid, we are convinced that any alternative model (of similar size) imposing no constraints at all will be much less realistic. In fact, this has been demonstrated by Amara et al. who found significantly different results for an unconstrained optimization of the active site in a vacuum and for an optimization including part of the protein backbone.[7f]

(20) Creighton, T. E. *Proteins: Structures and Molecular Properties*, 2nd ed.; Freeman: New York, 1993; p 12.

Results and Discussion

Basic Model of the Active Site. X-ray structures and XAS experiments indicate that the active site geometry remains almost unchanged throughout the various redox states.[3,5,6,21] This is particularly true for Ni-A and Ni-B. To account for this experimental fact and to prevent the structure from unreasonable geometric changes, one has either to include the protein environment in the computational model or to restrict the degrees of freedom in the optimization process. We chose the second option that has successfully been applied to metalloenzymes by Garmer and Krauss.[22] As will be shown, these constraints still permit a high flexibility of the dinuclear cluster; that is, differences of up to 0.4 Å are observed for the Ni−S bond lengths when the protonation state of the active site is varied despite the fixation of the methyl groups. For several of the discussed models, we also carried out optimizations with fewer constraints, but the results were not significantly different: for example, fixation of only one proton per methyl group (that one that substitutes for the Cα of the cysteine) gave Ni−S distances very similar to those reported later (average deviation 0.03 Å). Free optimization of the cyanide ligands, however, led to unreasonable changes because of the presence in the model of only one (Arg463) of three or four hydrogen bonds experimentally found to exist among these ligands and the protein environment.

(21) (a) Gu, Z.; Dong, J.; Allan, C. B.; Choudhury, S. B.; Franco, R.; Moura, J. J. G.; Moura, I.; LeGall, J.; Przybyla, A. E.; Roseboom, W. R.; Albracht, S. P. J.; Axley, M. J.; Scott, R. A.; Maroney, M. J. *J. Am. Chem. Soc.* **1996**, *118*, 11155−11165. (b) Davidson, G.; Choudhury, S. B.; Gu, Z.; Bose, K.; Roseboom, W.; Albracht, S. P. J.; Maroney, M. J. *Biochemistry* **2000**, *39*, 7468−7479.

(22) Garmer, D. R.; Krauss, M. *J. Am. Chem. Soc.* **1993**, *115*, 10247−10257.

Table 1. Calculated Interatomic Distances (Å) of Hydrogenase Active Site Models Including Arg463[a]

structure	Ni−Fe	Ni−O	Ni−S65	Ni−S68	Ni−S530	Ni−S533	Fe−O
μ-OH^- bridge (**1**)	2.86	1.89	2.22	2.37	2.23	2.45	2.03
μ-H_2O bridge	2.90	1.98	2.17	2.43	2.23	2.37	2.09
μ-OH^- bridge + H^+ on Cys65 (**2a**)	2.80	1.85	2.23	2.35	2.23	2.45	2.02
μ-OH^- bridge + H^+ on Cys68	2.96	1.88	2.16	2.67	2.16	2.40	2.01
μ-OH^- bridge + H^+ on Cys530 (**2b**)	2.77	1.89	2.21	2.29	2.27	2.48	2.02
μ-O^{2-} bridge (**3**)	2.80	1.80	2.28	2.38	2.25	2.57	1.90
μ-O^{2-} bridge + H^+ on Cys65	2.73	1.79	2.31	2.32	2.26	2.55	1.89
unbridged	2.79	-	2.21	2.34	2.22	2.19	-
unbridged + terminal OH^- at Ni	2.65	1.85	2.36	2.32	2.26	2.33	-
exptl data for Ni-A[b,c]	2.9 (2.9)	1.9 (1.8) [1.91]	2.2 (2.3)	2.5 (2.3)	2.3 (2.3)	2.5 (2.4)	2.2 (2.2)
exptl data for Ni−B[c]	[2.86]	[1.86]					

[a] Values taken from spin-restricted calculations with basis set A and the VWN functional. [b] Structural data are taken from the new refinement of X-ray data of the *D. fructosovorans* mutant.[18b] The originally reported values[18a] are given in parentheses. [c] Distances in square brackets are those from EXAFS analysis.[21b] Because only average Ni−S distances have been determined they are not included.

The positively charged guanido group of the highly conserved arginine residue Arg463 (see Figure 1) is included in all our models because we noticed that it significantly affects the position, and in certain cases even the binding mode, of the putative oxygen bridging ligand. We also found that residues other than Arg463 (e.g., Glu18 and His72) hardly affect the results of the geometry optimizations. There is, however, one residue that significantly interacts with the active site and that may be of importance for its electronic structure: His72, which is included in the *extended model*. It will be discussed later. For the examination of geometries and *g*-tensors, so as to carry out a first screening of possible Ni-A and Ni-B candidates, the *basic model* is sufficient.

We examine seven structures with a bridging and one with a terminal oxygen species in various protonation states as well as one structure with four-coordinated Ni that has been proposed to resemble Ni-B.[7c−e]

Geometric Structure. Strict comparison of experimental and calculated data is only possible for Ni-A, although various experimental findings indicate that the Ni-B structure is rather similar.[3,5,21] Table 1 lists selected bond lengths for nine optimized active site models and for the Ni-A state of the hydrogenase from the *D. fructosovorans* mutant. Of the seven possible Ni-A models (those with a bridging oxygen species), several show good agreement with the Ni-A X-ray data, considering the experimental error of 0.1−0.2 Å. Primarily, these are the models numbered **1**−**3**, although model **3** suffers from a very short Fe−O bond, but also, the other three models cannot be safely discarded on this basis only. Recent EXAFS experiments provide important additional data.[21b] In excellent agreement with the new crystallographic structure, a Ni−O distance of 1.91 Å has been determined for Ni-A (1.86 Å in Ni−B). Because the reported accuracy of these EXAFS values is considerably higher than that of the current crystallographic data, a bridging hydroxide is strongly favored over a bridging oxo or aquo ligand. Considering also the Ni−Fe distance, model **1**, which is unprotonated at all four cysteine sulfur atoms, shows the best agreement with the experimental data of Ni-A.

Very recently, Li and Hall also found that a μ-hydroxo-bridged structure with unprotonated cysteine groups is a likely candidate for Ni-A.[7g] However, from comparison with possible candidates for the Ni-SU state (EPR silent, unready) and the two Ni-SI states (EPR silent, ready), they concluded that Ni-A carries an additional proton at Cys65. Nevertheless, not only does this structure suffer from a short Ni−Fe distance (see Table 1 and also ref 7g) but also our calculations yield *g*-values that are not in good agreement with experiment as will be discussed later.

Table 2. Calculated *g*-Values of Hydrogenase Active Site Models Including Arg463[a]

structure	g_x	g_y	g_z
μ-OH^- bridge (**1**)	2.205	2.142	1.978
μ-H_2O bridge	2.145	2.109	2.000
μ-OH^- bridge + H^+ on Cys65 (**2a**)	2.230	2.105	1.992
μ-OH^- bridge + H^+ on Cys68	2.180	2.101	1.996
μ-OH^- bridge + H^+ on Cys530 (**2b**)	2.222	2.102	1.973
μ-O^{2-} bridge (**3**)	2.565	0.841	0.720
μ-O^{2-} bridge + H^+ on Cys65	2.644	1.450	1.366
unbridged	2.155	2.061	2.015
unbridged + terminal OH^- at Ni	2.118	2.048	2.005
exptl data for Ni-A[b]	2.31	2.23	2.01
exptl data for Ni−B[b]	2.33	2.16	2.01

[a] Values taken from spin-restricted calculations with basis set A and the VWN functional. [b] Values taken from ref 19a.

***g*-Tensors.** The calculated *g*-values are smaller than the experimental ones (but still within the limits found in the accompanying study[12]) for all optimized active site models in Table 2 except those with an oxo bridge for which they are completely unreasonable. At first sight, this seems to indicate that a μ-oxo-bridged structure is not a good model for the Ni-A or the Ni-B state.[23] However, one should consider the possibility that the effect of spin polarization, which we cannot include in our calculations of *g*-tensors, may have a stronger influence here: an oxo group may have a less contracted electron density distribution than a hydroxo or aquo ligand and be therefore more polarizable. Actually, significant spin polarization (and spin contamination, leading to $\langle S^2 \rangle$ values as high as 1.76) has been reported for the $S = {}^1/_2$ ground state of μ-oxo-bridged active site models in the literature when spin-unrestricted wave functions were used.[7f,g]

Nevertheless, Lubitz et al. proposed that an oxo-bridged structure resembles Ni-A, reporting calculated *g*-values of $g(x, y, z) = (2.37, 2.24, 1.98)$[24] and more recently (2.183, 2.159, 2.046).[7h] To our knowledge, their calculations include

(23) Preliminary calculations of *g*-values have shown that the replacement of the oxo bridge by a sulfido bridge leads to the same unsatisfying situation. See also ref 7i.

(24) Lubitz, W.; Stein, M.; Brecht, M.; Trofanchuk, O.; Foerster, S.; Higuchi, Y.; van Lenthe, E.; Lendzian, F. *Biophys. J.* **2000**, *78A*, 1660.

spin-polarization effects, although the computational details have not been reported and it is not clear why their original values have changed so much. However, the big difference between their values and ours is a clear indication that the electronic structure of model **3** should generally not be rated on the basis of spin-restricted (open-shell) calculations.[25] Therefore, we cannot discard at present model **3**. Instead, we will continue with the examination of the other models in Table 2 and return to model **3** later, in the discussion about the hyperfine and quadrupole coupling data.

A reasonable theoretical model for the two inactive states should be internally consistent in at least two ways. As pointed out in the accompanying study,[12] the underestimation of experimental values should be similar for g_x and g_y; that is, the relative errors for both values should not differ greatly.[26] Second, the experimentally observed differences between Ni-A and Ni-B should be well reproduced when comparing calculated *g*-values; that is, g_x should be somewhat smaller in the Ni-A model whereas g_y should be significantly smaller in the Ni-B model.

Table 2 contains only two possible models for Ni-A that match the first criterion. These are the hydroxo- and the aquo-bridged structure, both unprotonated at the cysteine sulfur atoms. The latter can be discarded because of the big relative error (>50%) for g_x and g_y (and also because of the long Ni−O bond shown in Table 1). On the other hand, the hydroxo-bridged model **1** not only shows good agreement with experimental bond lengths but also a relative error of just 35% for g_x and g_y. This error is of the same order as in the complexes in the accompanying study.[12] Model **1** is thus tentatively identified as Ni-A.

Using our second criterion, we can now look for a corresponding Ni-B model. Inspection of Table 2 shows that protonation of the hydroxo bridge leads to the required decrease of g_y but also to a large decrease of g_x. Therefore, the aquo-bridged structure can be ruled out. In contrast, protonation of a terminal cysteine (models **2a** and **2b**) has the desired effect of slightly rising g_x and significantly decreasing g_y. Particularly, model **2b**, which is protonated at Cys530, excellently reflects the experimental differences. The calculated decrease of g_y (−0.04) is smaller than in the experiment (−0.07), and this is exactly what one expects considering the relative error of 35%: a calculated shift of −0.045 would be expected, which is in very good agreement with the actual value. However, model **2a** still has to be considered as an alternative candidate for Ni-B because the calculated differences between models **2a** and **2b** are probably smaller than the error of the computational method. At least, **2a** is more likely to resemble Ni-B than Ni-A, in contrast to the findings of Li and Hall.[7g]

Four structures still remain to be discussed as possible candidates for Ni-B: hydroxo-bridged structures with protonated bridging cysteines and the two unbridged structures in Tables 1 and 2. Protonation of the bridging Cys68 yields a very large Ni−S68 distance that actually resembles a broken bond, and also a bigger Ni−Fe distance (Table 1). Both findings are not in agreement with recent XANES and EXAFS data, the latter suggesting a Ni−Fe distance of about 2.85 Å in Ni-B.[21b] Moreover, the calculated shifts of the *g*-values do not reflect the experimental shifts (Table 2). Because the protonation of Cys68 already resulted in such big shifts of the *g*-values, although S68 carries only a very small fraction of the spin density (see later), we did not consider a Cys533 protonated model to be a likely candidate for N-B. S533 carries a large part of the spin density (see later), and its protonation would have a dramatic effect on the *g*-values.

Unbridged structures also have been proposed to be likely candidates for Ni−B.[7c−e,27] However, there is experimental evidence against the four-coordinated unbridged structure in Table 2 because an oxygen species has been shown to be close to the Ni center by EPR,[28] ENDOR,[29] and EXAFS.[21b] Second, for both unbridged structures, rather small g_x- and g_y-values are calculated, whereas g_z is significantly bigger than in model **1**. Third, rather short Ni−Fe distances are obtained for both models, in particular for the one with a terminal hydroxo ligand, which again is not in agreement with EXAFS data.[21b]

Support for our assignment of Ni-A and Ni-B comes from the analysis of *g*-tensor orientations. For the Ni-A form of *D. vulgaris* hydrogenase, Trofanchuk et al. reported an angle ζ of 7−9° between the *z*-axis of the *g*-tensor and the Ni−S533 bond, whereas the g_x and g_y principal directions would roughly point toward S530 and S65, respectively.[11] In Ni-B, ζ has been found to be slightly bigger (11−16°), but overall, the orientation is quite the same. Although *D. vulgaris* hydrogenase is supposed to be structurally different from *D. gigas* and *D. fructosovorans* hydrogenases (e.g., the Ni−Fe distance is much bigger for the latter), the *g*-tensor orientation for models **1** and **2** agrees very well with these experimental data. Even the experimental finding that the angle ζ is slightly bigger in Ni-B is nicely reproduced. It increases from 4° in model **1** to 8° and 12° in models **2a** and **2b**, respectively. This is illustrated in Figure 2 where also the oxo-bridged model **3** is shown. As in the case of the two unbridged models (data not shown), the *g*-tensor orientation of model **3** is not in agreement with the experiment. For the latter, however, one must remember that the computed *g*-tensor orientation may be incorrect because of the relevance of spin polarization effects which have not been included in our calculation.

Hyperfine Coupling. The analysis of calculated geometrical data and *g*-values has left one good candidate for

(25) It should be noted, however, that spin polarization is not important for determining the geometric structure. We did not find any structural difference between the results of a spin-restricted and a spin-unrestricted geometry optimization of model **3**.

(26) See ref 12 for a definition of the relative error.

(27) (a) Huyett, J. E.; Carepo, M.; Pamplona, A.; Franco, R.; Moura, I.; Moura, J. J. G.; Hoffmann, B. M. *J. Am. Chem. Soc.* **1997**, *119*, 9291−9292. (b) Bleijlevens, B.; Faber, B. W.; Albracht, S. P. J. *J. Biol. Inorg. Chem.* **2001**, *6*, 763−769.

(28) Van der Zwaan, J. W.; Coremans, J. M. C. C.; Bouwens, E. C. M.; Albracht, S. P. J. *Biochim. Biophys. Acta* **1990**, *1041*, 101−110.

(29) Carepo, M.; Tierney, D. L.; Brondino, C. D.; Yang, T. C.; Pamplona, A.; Telser, J.; Moura, I.; Moura, J.; Hoffman, B. M. *J. Am. Chem. Soc.* **2002**, *124*, 281−286.

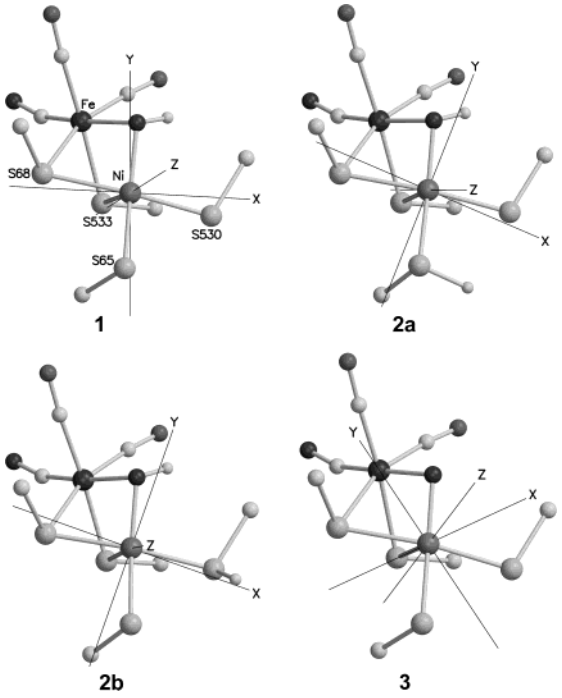

Figure 2. Schematic representations of optimized structures **1**, **2a**, **2b**, and **3** demonstrating the orientation of the *g*-tensor calculated in each case. For the sake of clarity, the methyl hydrogen atoms and the guanido group are not shown.

Ni-A and two for Ni-B which are shown in Figure 2. Ni-A is identified as a hydroxo-bridged cluster (**1**) whereas Ni-B carries an additional proton at one of the terminal cysteine groups while the hydroxo bridge is conserved (**2a** or **2b**). To find further evidence for our assignments and to decide whether model **3** resembles the Ni-A state, we carried out spin-unrestricted calculations on all models listed in Table 1 and obtained isotropic hyperfine coupling values a_{iso} that can be combined with *T*-tensors (anisotropic component of the hyperfine coupling) taken from spin−orbit calculations to yield A_i values.[12]

Unfortunately, in the few cases where experimental hyperfine coupling data have been reported, it was seldom taken into account that the orientations of the *g*- and *A*-tensors are not identical, which makes comparison of experimentally derived values with calculated data rather difficult (a discussion on this issue is included in the Supporting Information). ^{61}Ni data only have been published for Ni-A,[1b,30] whereas the coupling with ^{33}S was determined (incompletely) only for Ni-B.[31] Additionally, data for ^{17}O,[28,29] ^{57}Fe,[27a,29] and ^{1}H[32] have been reported, but the *A*-tensor was fully described only for ^{1}H (in both Ni-A and Ni-B) and ^{17}O (Ni-A). Moreover, we found that within the *basic model* the hyperfine couplings are significantly different from those obtained within the *extended model*, although the geometric structure and the *g*-values are practically identical within both models. Obviously, the calculated hyperfine coupling data are more sensitive toward additional weak interactions than are *g*-values and geometries. Still, the hyperfine coupling parameters calculated for the (basic) models listed in Table 1 (data not shown) confirm that only models **1**−**3** can be kept as reasonable candidates for the two oxidized states of the active site. Consequently, the following discussion will be limited to these four structures.

Extended Model of the Active Site. The interaction between the unpaired electron at the active site and a proximal nitrogen atom has been experimentally detected and analyzed for the Ni-A and Ni-C states of *D. gigas* hydrogenase[33] and the Ni-A and Ni-B states of *D. vulgaris* hydrogenase;[34] it has been ascribed to a histidine residue (His72 and His88 in *D. gigas* and *D. vulgaris* hydrogenase, respectively) close to the bridging sulfur atom of Cys533 (Cys549 in *D. vulgaris*). This indicates a relevant influence of that histidine with respect to the electronic spin distribution of the active site that should be taken into account in any advanced computational model. All structures discussed in following paragraphs were thus reoptimized including the imidazole ring of His72, which was fixed at the γ-carbon atom as shown in Figure 1. This ensures that the distance between S533 and Nϵ, which is most important for the interaction between the imidazole ring and the active site, is not greatly changed during the optimization process whereas the orientation and the geometry of the ring are allowed to be optimized freely. Because the protonation state of this histidine had not been determined experimentally, this question was addressed first.

Protonation State of His72. We chose our Ni-A model **4** to study the effect of the imidazole group in its three possible protonation states: protonated at Nδ, protonated at Nϵ, and doubly protonated. We optimized the three structures but found little difference between the resulting active site geometries. Only the geometry of the imidazole ring was significantly affected by protonation/deprotonation, although its orientation was essentially conserved during the optimization. Table 3 includes *g*-values taken from calculations with either a local (VWN) or a gradient-corrected (BP) density functional. We tried both because when a proton is placed at Nϵ of His72 it will point directly toward S533 with a S−H distance of about 2.1 Å, corresponding to a weak hydrogen bond; it is well-known that a correct description of hydrogen bonds and other weak interactions requires the use of gradient corrected density functionals.[35] The effect is clearly demonstrated in Table 3. For the model without His72 and that with the imidazole ring singly protonated at Nδ, similar *g*-values are obtained with and without gradient correction.

(30) (a) Albracht, S. P. J.; Graf, E.-G.; Thauer, R. K. *FEBS Lett.* **1982**, *140*, 311−313. (b) Kojima, N.; Fox, J. A.; Hausinger, R. P.; Daniels, L.; Orme-Johnson, W. H.; Walsh, C. *Proc. Natl. Acad. Sci. U.S.A.* **1983**, *80*, 378−382.
(31) Albracht, S. P. J.; Kröger, A.; van der Zwaan, J. W.; Unden, G.; Böcher, R.; Mell, H.; Fontijn, R. D. *Biochim. Biophys. Acta* **1986**, *874*, 116−127.
(32) (a) Fan, C.; Teixeira, M.; Moura, J.; Moura, I.; Huynh, B.-H.; LeGall, J.; Peck, H. D., Jr.; Hoffman, B. M. *J. Am. Chem. Soc.* **1991**, *113*, 20−24. (b) Gessner, C.; Stein, M.; Albracht, S. P. J.; Lubitz, W. *J. Biol. Inorg. Chem.* **1999**, *4*, 379−389.
(33) Chapman, A.; Cammack, R.; Hatchikian, C. E.; McCracken, J.; Peisach, J. *FEBS Lett.* **1988**, *242*, 134−138.
(34) Brecht, M.; Stein, M.; Trofanchuk, O.; Lendzian, F.; Bittl, R.; Higuchi, Y.; Lubitz, W. In *Magnetic Resonance and Related Phenomena*; Technische Universität Berlin: Berlin, 1998; Vol. II, pp 818−819.
(35) Wie, D.; Proynov, E. I.; Milet, A.; Salahub, D. R. *J. Phys. Chem. A* **2000**, *104*, 2384−2395.

Table 3. Effect of the Inclusion of His72 on the Magnetic Resonance Parameters of Ni-A Model **1**

structure	method	*g*-values g_x	g_y	g_z	quadrupole coupling [MHz] ^{14}N (Nϵ of His72)
without His72	VWN[a]	2.205	2.142	1.978	
	BP[a]	2.189	2.141	1.987	
His72 protonated at Nδ	VWN[a]	2.176	2.123	1.991	
	BP[a]	2.165	2.121	1.995	(0.96, 0.99, −1.95)
	BP[b]				(1.15, 1.18, −2.33)
His72 protonated at Nϵ	VWN[a]	2.243	2.152	1.947	
	BP[a]	2.214	2.158	1.970	(0.37, 0.65, −1.02)
	BP[b]				(0.36, 0.77, −1.13)
His72 protonated at Nδ and Nϵ	VWN[a]	2.333	2.066	1.804	
	BP[a]	2.274	2.140	1.895	(−0.06, −0.66, 0.72)
	BP[b]				(−0.21, −0.65, 0.86)
Ni-A[c]	exptl	2.31	2.23	2.01	±(−0.31, −0.64, 0.95)[33]

[a] Values taken from spin-restricted spin−orbit calculations with basis set A. [b] Values taken from spin-unrestricted calculations using basis set B′ for Nϵ and basis set A for all other atoms. [c] *g*-Values taken from ref 19a.

For the two models with His72 protonated at Nϵ, the BP functional performs significantly better than VWN, the latter largely overestimating the interaction between S533 and His72. The best overall agreement with experimental *g*-values is obtained for the structure with a neutral imidazole protonated at Nϵ using the gradient corrected functional.

Another very sensitive probe of the protonation state of the imidazole group is the quadrupole interaction with Nϵ. Experimentally, the values $e^2qQ/h = 1.90$ MHz and $\eta = 0.34$ have been found for Ni-A.[33,34] This corresponds to a tensor with principal values $P(1, 2, 3) = \pm(-0.31, -0.64, 0.95)$ MHz.[36] In Table 3, values taken from spin−orbit calculations (with basis set A)[12] and from spin-unrestricted calculations (with basis set B′)[12] are reported. From the calculations performed on $[Ni(mnt)_2]^-$, we know that basis set A leads to an underestimation of the quadrupole interaction because of the frozen core approximation.[12] Nevertheless, the structure with an uncharged imidazole, protonated at Nϵ, yields quite good agreement with experiment when basis set A is used, whereas basis set B′ yields significantly bigger values. On the other hand, the values calculated for the doubly protonated structure are clearly too small, regardless of the basis set quality. Thus, we conclude that the actual situation in the enzyme is intermediate between a neutral and a positively charged His72: that is, His72 is singly protonated at Nϵ but has an additional hydrogen bridge interacting with Nδ. This is in full accordance with crystallographic data which show a second histidine (His486 in *D. gigas*) with its Nϵ at the appropriate distance for hydrogen-bonding to Nδ of His72.[3] Considering the calculated *g*-values and quadrupole couplings given in Table 3, it seems more adequate to model His72 as an uncharged imidazole ring protonated at Nϵ than to model it as a doubly protonated structure. Consequently, all models discussed in following paragraphs contain such an uncharged imidazole group.

(36) The following relations apply for ^{14}N: $e^2qQ/h = 2P_3$; $\eta = |(P_1 - P_2)/P_3|$.

Geometric Structure. The results of the optimizations carried out on models **1′**−**3′** (the same as **1**−**3** but with the imidazole group protonated at Nϵ) demonstrate once more that the inclusion of residues other than Arg463, His72 in this case, does not significantly affect the active site geometry, despite the interaction between S533 and Nϵ of the imidazole.[37] The hydroxo-bridged model **1′** still shows the best agreement with the experimental data of Ni-A, most clearly demonstrated by the Ni−O and Ni−Fe distances. The big deviation from experiment found for the Fe−O distance indicates once more that model **3′** is not a good Ni-A candidate.

It should be noted that the results obtained with models **1′** and **2b′** are not in full agreement with the trends in C−O bond lengths deduced from the experimentally determined IR stretching frequencies of the carbonyl ligand in Ni-A and Ni-B. This bond length is supposed to depend largely on the charge density on the Fe atom and, thus, also on the overall charge of the active site. Accordingly, a significant shift (+20 cm^{-1}) is observed in the IR when the EPR-silent species Ni−SI_{1914} gets protonated, forming Ni−SI_{1934}.[2] On the other hand, the experimental difference between Ni-A and Ni-B is only 1 cm^{-1}, suggesting the same overall charge for both oxidized states, whereas model **1′** is more negatively charged than model **2b′**. Not surprisingly, we found a significantly shorter C−O bond (corresponding to a higher IR frequency) for model **2b′** when we optimized both models without constraints for the carbonyl ligand. However, the actual situation in the enzyme may be such that a charge difference between the Ni-A and Ni-B states of the active site is compensated by other charged residues close to the dinuclear cluster. A reasonable schematic model, which includes such a charge compensation, will be presented later.

Other Weak Interactions. In view of the effects of the histidine residue on the *g*-values observed in Table 3 (and also the problem of charge compensation), it would seem desirable to examine larger parts of the protein environment and include all possibly interacting residues into the computational model. However, this would dramatically increase computation time if carried out in a pure quantum mechanical way. Alternatively, we have included the electrostatic effects of the protein environment into our calculations via the COSMO approximation in order to model the active site as correctly as possible without introducing more atoms. Although this is a rather primitive approach, the quality of the computational model should be significantly better when the active site is calculated in a dielectric continuum rather than in a vacuum. Following Pavlov et al.,[7b] we choose the dielectric constant ϵ to be equal to 4, which is an average value for proteins. All results presented and discussed later include the dielectric effects of the protein, those from the spin-unrestricted calculations as well as those from the spin-restricted spin−orbit calculations. We also verified for Ni-A model **1′** that the geometric structure is not significantly affected by the inclusion of dielectric effects (data not shown) and, consequently, did not reoptimize again models **1′**−**3′**.

(37) A table with calculated distances is included in the Supporting Information.

Table 4. Calculated *g*-Values, Spin Densities, and Quadrupole Couplings of Active Site Models Including Arg463, His72 (protonated at Nϵ), and Dielectric Effects[a]

	g-values[b]			spin densities[c]							quad. coup. [MHz][c]
model	g_x	g_y	g_z	Ni	O	Fe	S65	S68	S530	S533	^{14}N (Nϵ of His72)
1′	2.213	2.168	1.982	0.65	0.02	−0.01	0.01	0.00	0.03	0.27	(0.34, 0.74, −1.08)
2a′	2.210	2.140	1.993	0.61	0.03	0.00	0.02	−0.02	0.04	0.31	(0.44, 0.75, −1.18)
2b′	2.233	2.126	1.982	0.63	0.02	0.01	0.02	−0.01	0.00	0.31	(0.42, 0.75, −1.17)
3′	2.928	0.876	0.749	0.59	0.23	−0.01	−0.01	0.02	−0.01	0.14	(0.14, 0.76, −0.90)
Ni-A	2.31	2.23	2.01								±(−0.31, −0.64, 0.95)[33]
Ni-B	2.33	2.16	2.01								±(−0.31, −0.68, 0.99)[33]

[a] Dielectric effects were modeled with COSMO using the dielectric constant $\epsilon = 4$. [b] Values taken from spin-restricted spin−orbit calculations with basis set A and BP gradient correction. [c] Values taken from spin-unrestricted calculations using basis set B′ (for Ni, Fe, O, and S) and BP gradient correction.

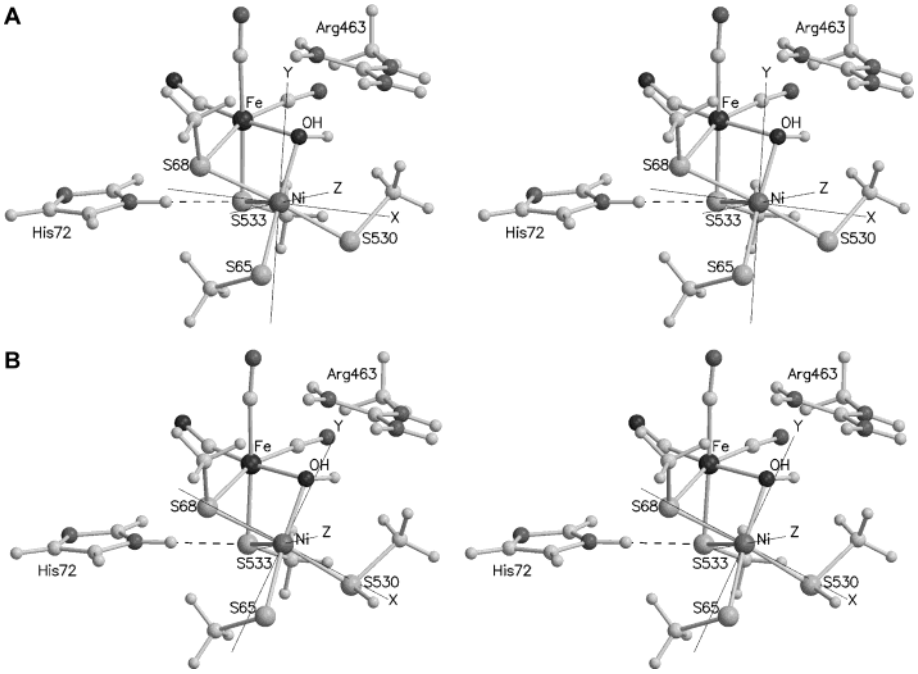

Figure 3. Stereoviews (crossed eyes) of models **1′** and **2b′** including the *x*-, *y*-, and *z*-axes of the calculated *g*-tensors. (A) Ni-A model **1′**; (B) Ni-B model **2b′**.

***g*-Tensors.** Table 4 shows that, from the point of view of *g*-values, models **1′** and **2b′** are confirmed as good candidates for Ni-A and Ni-B: g_z is now calculated to be equal for both, in excellent agreement with experiment. Also, the experimental differences of g_x and g_y between Ni-A and Ni-B are almost quantitatively reflected: the increase of g_x is only slightly bigger than expected whereas the decrease of g_y is slightly smaller. Moreover, it turns out that model **2a′** is no longer a likely model for Ni-B: the difference between g_x and g_y is only 0.07 and thus not significantly bigger than in Ni-A model **1′**. Obviously, we still must consider that the electronic structure of model **3′** is not well described in the spin-restricted calculation; it should thus not be rated on the basis of the calculated *g*-values in Table 4.

The orientation of the *g*-tensors is very similar to that found for the smaller models **1**−**3**, and thus, the results obtained for Ni-A and Ni-B models **1′** and **2b′**, illustrated in Figure 3A,B, respectively, are in very good agreement with experiment.

Spin Distribution. Table 4 also reports the calculated spin densities at the two metal centers and the five ligand atoms around nickel. For all models, except the oxo-bridged one, the spin density is practically localized at the Ni atom (mainly in the d_{z^2} orbital) and the sulfur of Cys533 whereas the bridging oxygen atom carries very little spin density, just enough to explain the ^{17}O hyperfine couplings observed in Ni-A and Ni-B.[28,29] Only in model **3′** is a high spin density found at the oxygen bridge, and this is a strong argument against this structure because Ni-A and Ni-B show ^{17}O hyperfine couplings of similar magnitude.

Interestingly, we did not find large negative spin densities for model **3′**, which indicates that in our calculation spin polarization is less important than previously reported in the literature for μ-oxo-bridged active site models.[7f,g] The ADF program does not permit the calculation of the expectation value $\langle S^2 \rangle$, but we deduce from the absence of such negative spin densities that spin contamination is also likely to be less important for our model. Very recently, it was also shown by Stein et al. that oxo-bridged structures can be calculated without having significant spin contamination.[7i] Thus, we may trust the calculated isotropic hyperfine coupling values discussed later equally well for all models including model **3′**.

Hyperfine Coupling. Having discarded model **2a′**, we still have to verify if models **1′** and **2b′** are in agreement with experimental hyperfine coupling data, and if additional

arguments may be found against model **3′**. However, analysis of the obtained data is not at all straightforward because direct comparison of experimental and calculated hyperfine values in most cases is impossible because of the noncoincidence of *g*- and *A*-tensor axes. Therefore, here we will only summarize the most important findings. A full listing of the values obtained, and a thorough discussion of them and of the consequences of noncoincident tensor axes, is available as Supporting Information.

Calculated *T*-tensors for model **1′** are in reasonable agreement with experimental data of Ni-A. Moreover, the isotropic components a_{iso} (in particular $a_{iso}(^{17}O)$), which are computed to be significantly different for models **1′** and **3′**, support our assignment of a hydroxo-bridged Ni-A form. For Ni-B, comparison of calculated and experimental *T*-tensors does not really clarify the situation because the deviation from experiment is bigger than the observed differences between the computational models. However, the small difference experimentally found between the isotropic hyperfine coupling of protons H_1 and H_2 (at Cβ of Cys533) in Ni-B is best reproduced by model **2b′**, confirming our earlier assignment.

Quadrupole Coupling. The data compiled in Table 4 give further strong evidence against model **3′**, that is, against a μ-oxo bridge in Ni-A: the ^{14}N quadrupole coupling of Ni-A is much better reproduced in the hydroxo-bridged model **1′**. In fact, for the latter, the calculated values are slightly higher than the experimental data but, as pointed out previously, this can easily be explained by the missing hydrogen bridge between Nδ and a neighboring imidazole ring which has not been included in our models. Obviously, this makes model **3′** even less favorable because here inclusion of the hydrogen bridge will lead to a decrease of the already small values P_i.

Comparison with NiFeSe Hydrogenases. Additional support for our Ni-B model **2b′** comes from data for the selenium containing enzyme *Methanococcus voltae*. Usually, NiFeSe hydrogenases only show the Ni-C signal but no Ni-A or Ni-B signals.[38] However, Sorgenfrei et al. recently reported the EPR spectrum of an oxidized sample of that enzyme that was proposed to originate from the Ni-B state, and although it was isotopically enriched with ^{77}Se, no hyperfine splitting or line broadening was found.[39] This is an important finding because the nuclear magnetic moment of ^{77}Se is about seven times stronger than that of ^{33}S, giving thus seven times higher hyperfine couplings at equal spin densities. Crystallographic data show that the selenium atom is a ligand to nickel, substituting for the sulfur atom in Cys530.[6b] Therefore, it must be concluded that the selenium nucleus does not "feel" any spin density in Ni-B (provided that the spectrum observed by Sorgenfrei et al. indeed is that of a Ni-B form, which was not definitely proven). Model **2b′** is in perfect agreement with that. Protonation of the Cys530 ligand completely removes from the sulfur atom the small spin density that is observed for the unprotonated forms (Table 4), and the calculated principal values of the *A*-tensor of $^{33}S530$ are significantly smaller in model **2b′** than in model **1′** (data not shown).

Activation Mechanism. From the point of view of geometric and electronic structure, we seem to have identified Ni-A and Ni-B, but there is one important question left: can models **1′** and **2b′** help to explain the kinetic data? Ni-B, which is also called the ready state, is much more rapidly activated than Ni-A (unready state).[10] It is quite established that part of the activation process consists of the removal of the bridging oxygen species,[8,21b] and consequently, crystallographic structures of activated enzyme states show neither bridging nor terminal oxygen ligands at the Ni site.[6] Therefore, it is tempting to speculate that the lower activation energy of Ni-B is the result of a weaker binding of the bridging species.[7g,11] Without doubt, this is most easily achieved by (further) protonation of the bridging ligand. In fact, in some moment, it needs to be protonated to be able to leave as a water molecule. However, a model in which a different protonation state of the bridging ligand is the only significant difference between Ni-A and Ni-B does not explain why both forms are not in equilibrium; neither the hydroxo-bridged model **1′** nor the aquo-bridged model satisfactorily reproduces all experimental data of Ni-B as pointed out previously. A better explanation of the kinetics could be given if Ni-B already had lost the bridging oxygen species. Because an oxygen atom has been shown to interact with the active site in Ni-B,[28] it would then have to be bound terminally, for example, as a hydroxo ligand to Ni as recently proposed by Bleijlevens et al.[27b] However, this possibility is not in agreement with the presented data from our calculations, particularly the *g*-values and the Ni−Fe distance, which is then much shorter than that determined by EXAFS analysis.

Blocking of the proton channel could also be responsible for the slow activation of Ni-A/Ni-SU: no significant difference has been found comparing ENDOR spectra of Ni-A in H_2O and D_2O which means that none of the protons detected is exchangeable.[32a] On the other hand, for Ni-B, an exchangeable proton has been reported and tentatively assigned to a proton of a hydroxo or aquo group. However, we would like to point out that this H/D exchange was detected after activation and reoxidation of the enzyme in D_2O, not by simple solvation of Ni-B in D_2O. Thus, these ENDOR experiments neither prove that the proton channel is functional in Ni-B nor that it is blocked in Ni-A. In fact, there is experimental evidence that the active site (and this does not necessarily mean the bridging oxygen species) can be easily protonated after reduction of Ni-A to Ni-SU (silent unready state),[2] indicating a working proton channel. Although our calculations on model **1′** indicate that the hyperfine coupling of the hydroxo proton is strong enough to be visible (data not shown), and thus, it should correspond to one of the (unassigned) protons detected by ENDOR, the hydroxo group may well be isolated from the proton channel. We conclude that protons do not reach the bridging oxygen species in Ni-A, but this may not be the principal reason for the slow activation process.

(38) Teixeira, M.; Fauque, G.; Moura, I.; Lespinat, P. A.; Berlier, Y.; Prickril, B.; Peck, H. D., Jr.; Xavier, A. V.; LeGall, J.; Moura, J. J. G. *Eur. J. Biochem.* **1987**, *167*, 47−58.
(39) Sorgenfrei, O.; Duin, E. C.; Klein, A.; Albracht, S. P. J. *Eur. J. Biochem.* **1997**, *247*, 681−687.

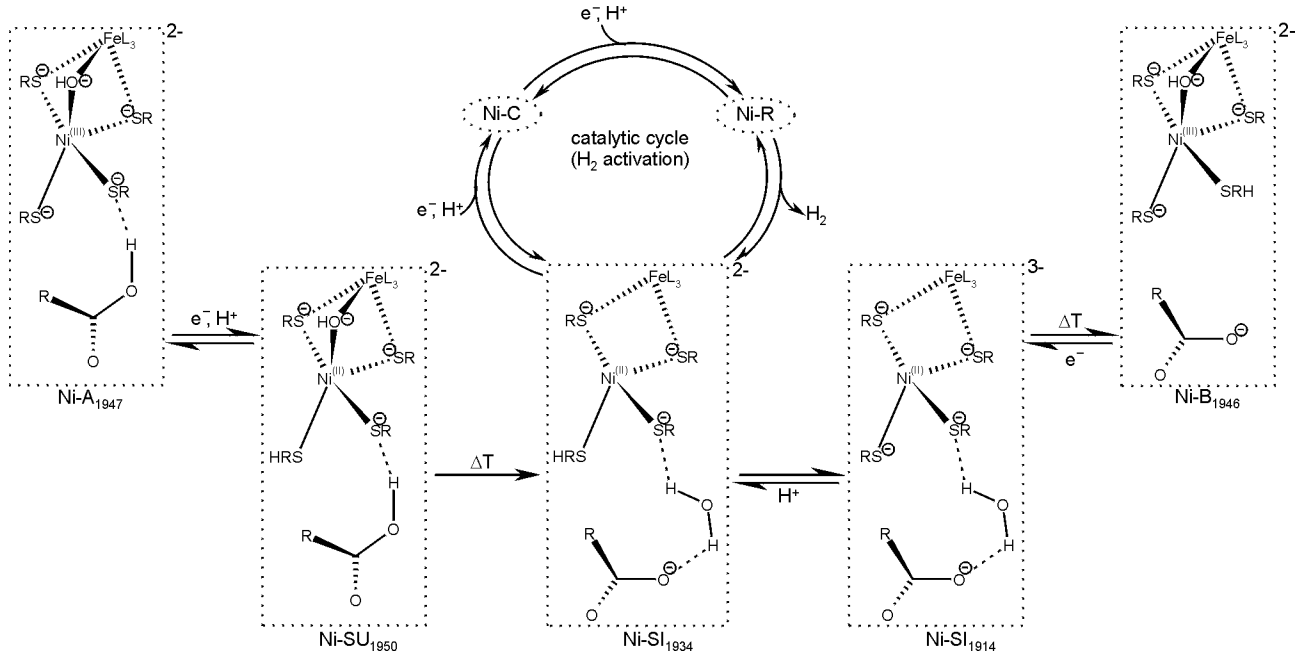

Figure 4. Schematic model describing possible activation processes for Ni-A and Ni-B. The experimentally determined IR frequency of the CO ligand is printed as subscript to each state, and on the top right corner of each dotted box, the overall charge is given. The RCO_2-fragment represents the Glu18 residue, and FeL_3 represents $[Fe^{II}(CO)(CN)_2]$.

We favor an alternative explanation for the different behavior of Ni-A and Ni-B that is based on a different ability to (temporarily) store the water molecule that is likely to leave the active site during the activation process. We think that rather small changes in the position of Cys530 and the closely located Glu18 could give rise to such differences. A working model that we propose here for future studies is presented in Figure 4, which shows schematic structures of the active site, including part of Glu18. It is still a rather speculative model, based on the presented results for Ni-A and Ni-B and preliminary calculations on several possible candidates (not only the shown ones) for the three EPR-silent states Ni-SU, Ni-SI_{1934}, and Ni-SI_{1914}, but it accounts for practically all available experimental data described in the following paragraphs.

(1) IR Frequencies. In Figure 4, the overall charge is equal in all states but Ni-SI_{1914}, which has the lowest IR frequency of all states characterized so far.[2] The charge compensation through the unprotonated glutamic acid in Ni-B (possibly along with slight changes in the environment of the iron center) may thus resolve the problem posed by the different C−O bond lengths found for models **1′** and **2b′**, which did not include that glutamic acid residue.

(2) EXAFS Results. Only in forms A, B, and SU has oxygen been found to be a ligand to Ni, with a Ni−O bond length of about 1.9 Å which is best reproduced by bridging hydroxo ligands.[21b] For Ni-SU, this is confirmed by a geometry optimization of the structure shown in Figure 4 whereas our optimizations of alternative structures indicate that neither a terminal nor a bridging water ligand coordinates to Ni(II) in that state because of electronic and/or steric impediments (results to be reported in a forthcoming paper). A significantly shorter Ni−Fe distance has been reported for Ni-SI (probably Ni-SI_{1934} because it was prepared at low pH) than for Ni-A and Ni-B. Preliminary results show that the geometry calculated for the Ni-SI_{1934} model in Figure 4 is in good agreement with that (Ni−Fe = 2.65 Å), whereas a significantly longer Ni−Fe distance (2.80 Å) is predicted for the corresponding Ni-SI_{1914} model.

(3) Redox and Protonation Equilibria. Most of the equilibria shown in Figure 4 are well established, in particular, that between Ni-SI_{1914} and Ni-SI_{1934}, which differ by one proton.[2] The reduction of Ni-B to a mixture of the two Ni-SI forms is pH dependent, but less than one proton (in the average) has been calculated to enter the active site. Therefore, it is likely that in a first step a simple one-electron reduction from Ni-B to Ni-SI_{1914} occurs before protonation and reorganization yields Ni-SI_{1934}. This is also in agreement with the mentioned decrease of the IR frequency during reduction. As pointed out previously, the proton involved in the Ni-A/Ni-SU transition is likely to be bound to a terminal cysteine rather than to the bridging hydroxo group.

(4) Kinetic Barriers. The transformation from Ni-SU to Ni-SI (to which of the two SI states has not been determined experimentally) is very slow, and at least in the absence of O_2, it is irreversible. In our working model, this is mostly due to a reorientation of the Glu18 residue and possibly also of Cys530. It may be significant that in recent crystal structures Glu18 shows relatively high temperature factors compared to its environment, and that Cys530 displays conformational flexibility,[5b,18b] although the redox states corresponding to the less populated conformers remain unclear. The oxidation of the Ni-SI states to Ni-B is also a slow process[2,40] which might be due to some steric hindrance of the incorporation of the bridging hydroxo ligand.

(40) Coremans, J. M. C. C.; van der Zwaan, J. W.; Albracht, S. P. J. *Biochim. Biophys. Acta* **1992**, *1119*, 157−168.

Note that the exact location and binding mode of the water molecule may be significantly different from that given in the schematic presentation of Figure 4. For example, in Ni-SI_{1934}, the water molecule may already have moved further away, liberating Glu18 for acceptance of protons from the active site. Without doubt, many aspects of our model still need to be confirmed by further computational studies, requiring the modeling of the active site together with large parts of the protein environment. This is definitely beyond the scope of the method presented in this work and must be done by a hybrid QM/MM method that combines quantum mechanics and molecular mechanics.[41]

Conclusion and Outlook

In this study, we do not attempt to predict in full (which would require the inclusion of large parts of the protein backbone in the model) structural details of the active site of NiFe hydrogenases but rather to elucidate aspects not deducible from the diffraction data. This is done by searching how to best reproduce sensitive spectroscopic properties while conforming to experimentally verified structural parameters: hence, the fixation of some atoms in the geometry optimizations. Inclusion of the positively charged arginine residue already in our basic model is necessary so that the position of any ligand that is bridging the dinuclear cluster (a key feature of the active site) is modeled correctly. However, to model accurately the electronic structure and to reproduce the paramagnetic properties of the active site, also the interaction with His72 must be considered. Our extended model thus includes an imidazole group, and also, we take the dielectric effect of the protein environment into account.

Analysis of the calculated *g*-values as well as of the *g*-tensor orientations leaves only one pair of structures that reflects well the experimental differences between Ni-A and Ni-B. Both structures are μ-hydroxo-bridged. Ni-A (model **1′**) is singly protonated at the bridging oxygen but unprotonated at the four cysteine ligands. The assignment of Ni-B (model **2b′**) has been somewhat more difficult. From experimental data (EXAFS, XANES, EPR), it seems quite clear that Ni-B is a five-coordinated Ni(III) species with one oxygen ligand and that its electronic structure is not very different from that of Ni-A. The only model that satisfactorily reproduces all these data, including those from ENDOR spectroscopy, is model **2b′**.

To the best of our knowledge, we are the first to present a detailed model that may explain the puzzling question why Ni-A and Ni-B apparently are so similar in terms of structural and spectroscopic properties but so different regarding their activation. Our model takes into account virtually all experimental data available in the literature, and it is fully supported by our calculations on Ni-A, Ni-B, and the corresponding reduced forms.

The extensive calculations on possible Ni-A and Ni-B models clearly demonstrate the merit, but also the limits, of the computational method used in this work. Now that we have learned which parts of the active site and its environment are necessary for the accurate description of the active site's geometric and electronic structure, we will extend our studies to other paramagnetic states of the active site. A better description of the structural parameters of the active site will be achieved by inclusion of parts of the protein backbone, using a hybrid method (which combines the DFT method used in this work and molecular mechanics)[42] that has recently been made available within the ADF program package. Also, work is in progress to obtain crystal structures of the Ni-B and Ni-SI_{1934} states in pure form. By combining computational and experimental results, we hope to be able to refine our picture of the activation/inactivation processes as well as to propose a mechanism for the CO inhibition. This might finally lead to a better understanding of the hydrogen activation mechanism in NiFe hydrogenases.

Acknowledgment. This research was supported by Grant BIO4-98-0280 from the European Union BIOTECH program and Grant BQU2000-0991 from the Spanish Ministerio de Ciencia y Tecnología (MCYT). C.S. thanks the German Academic Exchange Service (DAAD) for a postdoctoral fellowship, and A.L.D., the MCYT for a "Ramon y Cajal" contract. We thank Dr. Arnd Müller for helpful discussions. We also thank Prof. C. Hatchikian for providing experimental data prior to publication and Prof. M. Hall for helpful comments.

Supporting Information Available: X-ray structural data of the active site of the *D. fructosovorans* mutant as used in the calculations, coordinates of optimized models **1′** and **2b′**, table of calculated interatomic distances for models **1′**, **2a′**, **2b′**, and **3′** (CIF); detailed discussion of experimental and computed hyperfine coupling data (PDF). This material is available free of charge via the Internet at http://pubs.acs.org.

IC020016L

(41) Amara, P.; Field, M. J. In *Computational Molecular Biology*; Leszczynski, J., Ed.; Elsevier Science: Amsterdam, 1999; pp 1−33.

(42) Woo, T. K.; Cavallo, L.; Ziegler, T. *Theor. Chem. Acc.* **1998**, *100*, 307−313.